RSC Advances

ROYAL SOCIETY OF CHEMISTRY

www.rsc.org/advances

Graphical abstract

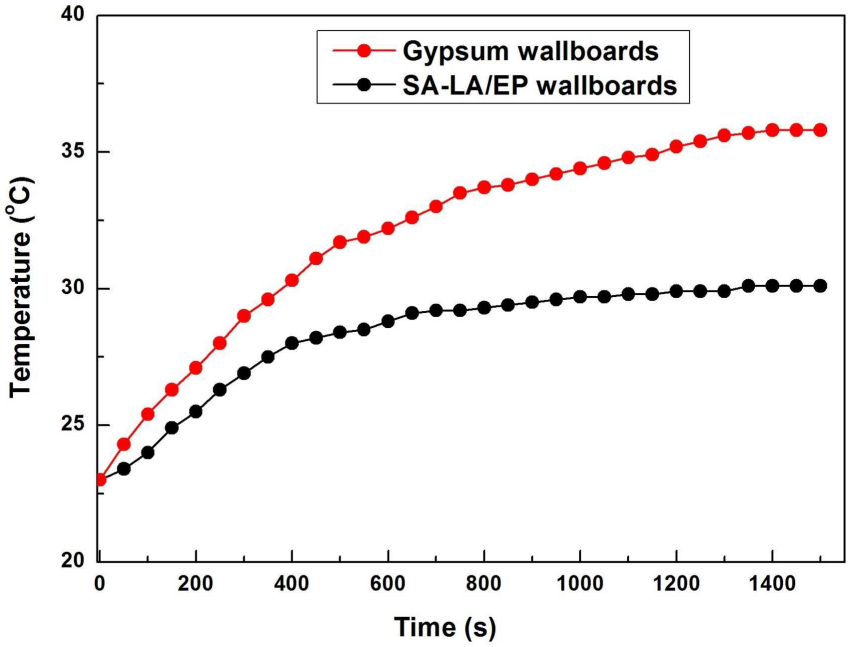

Journal Name

RSCPublishing

PAPER

Acid-hybridized expanded perlite as a composite phase-change material in wallboards

Cite this: DOI: 10.1039/x0xx00000x

Kang Peng [a,b], Jinyi Zhang [a,b], Huaming Yang [a,b,c,*], Jing Ouyang [a,b,*]

Received ooth January 2012,
Accepted ooth January 2012

DOI: 10.1039/x0xx00000x

www.rsc.org/

Form-stable composite phase change materials (PCMs) for use in wallboards were prepared by absorbing stearic acid (SA) and lauric acid (LA) eutectic mixtures into the pores of expanded perlite (EP) via vacuum impregnation. The microstructure, thermal properties and the thermal reliability of the composite PCMs were characterized by thermogravimetric and differential scanning calorimetry, X-ray diffraction, Fourier transform infrared spectroscopy, and scanning electron microscopy. The results indicate that the maximum SA-LA absorption of the EP was as high as 65 wt.% without any melted SA-LA leakage. The latent heat of the composite PCMs was 119.0 J/g at its melting temperature of 31.69 °C and 117.4 J/g at its freezing temperature of 30.01 °C, respectively. A thermal cycling test showed that the composite PCMs have excellent structural stability and thermal reliability after 100 melt-freeze cycles. A gypsum-based building wallboard containing 6 wt.% SA-LA/EP had a low density (0.924 g/cm^3), high mechanical strength (2.19 MPa), and remarkable heating preservation performance. These properties indicate that the composite PCMs that we used for wallboards can be considered an efficient heating preservation material for practical applications in building energy conservation.

1. Introduction

Rapidly growing, world energy consumption has caused various problems such as the depletion of energy resources and supply difficulties, and it is a heavy environmental burden[1]. The energy consumption of commercial and residential buildings accounts for 20–40% of the total amount[2]. This is mainly related to climate, building material selection, architectural design, and energy systems[3, 4]. As the demand for thermal comfort in buildings increases, heating ventilation and air conditioning (HVAC) have become necessities[5]. This is responsible for the high energy consumption in the residential and non-residential sectors[6, 7]. To reduce the energy consumption of HVAC systems, heating and cooling loads need to be shifted from peak to off-peak periods using phase change materials (PCMs)[8]. PCMs are latent heat thermal energy storage (LHTES) materials which play an important role in building energy conservation. They store significant amounts of thermal energy in the building envelope without the burden of structural mass, which reduces the indoor temperature swing [9-11].

Several PCMs including inorganic and organic PCMs have been widely investigated for use in LHTES [12-14]. The use of inorganic PCMs such as salt hydrates and alloys is limited because of subcooling and phase separation during phase change processes[15]. Organic PCMs such as fatty acids, paraffins, and their mixtures are considered to be promising PCMs because of their excellent thermal performance, stable chemical and thermal properties, non-corrosive nature, nontoxicity, and little or no subcooling[16]. Fatty acid eutectic mixtures are normally used as efficient PCMs in building energy conservation because of their high latent heat capacity and their tunable phase change temperature upon changing the eutectic ratio. However, the leakage of organic PCMs in the melting process limits their application to some extent[17-19]. To prevent this leakage, form-stable PCMs have been developed by the encapsulation of PCMs into supporting materials. These materials can retain melted PCMs. Common supporting materials include polymers, porous materials, and minerals such as polyethylene[20, 21], polymethyl methacrylate[22, 23], expanded graphite[24, 25], expanded perlite[26], expanded vermiculite[27], diatomite[28], kaolinite[29] and bentonite[30]. Many other porous minerals (such as zeolite[31], sepiolite[32], wollastonite[33] and coal-series kaolinite[34]) are suitable for preparation of composite PCMs. These porous minerals could enhance structural and chemical stability of composite PCMs. The amount of embeddable PCM depends on the porous features. The expanded perlite has enormous advantages for its appropriate pore size distribution and high pore volume.

Expanded perlite (EP) is a porous amorphous silica mineral and is obtained when expanding perlite by rapid heating to 700–1200 °C[35]. EP is used widely in walls as an economical and efficient

[a] *Centre for Mineral Materials, School of Minerals Processing and Bioengineering, Central South University, Changsha 410083, China*

[b] *Key Laboratory for Mineral Materials and Application of Hunan Province, Central South University, Changsha 410083, China*

[c] *State Key Laboratory of Powder Metallurgy, Central South University, Changsha 410083, China*

**Corresponding author, email: hmyang@csu.edu.cn, jingouyang@csu.edu.cn,Tel.: +86-731-88830549, Fax: +86-731-88710804.*

insulation material because of its low density, its sound absorption ability, and its flame retardance ability[36]. Therefore, EP composite PCMs have advantages in terms of thermal insulation and heat storage capacity and they can be used as energy-efficient building materials. Several EP composite PCMs have been reported for use in thermal energy storage, such as lauric acid/expanded perlite[26], paraffin/expanded perlite[37-39] and Lauric–palmitic–stearic acid/expanded perlite composite[40]. However, the practical applications of EP composite PCMs in building energy conservation still needs more research about physical and thermal properties of building materials. Two general methods have been proposed for the application of composite PCMs to building materials: (1) dry mixing PCMs and binding materials such as gypsum and cement to obtain mortars[41] and (2) the incorporation of building materials into PCMs to obtain wallboards or blocks[42]. The second method is simple and convenient in practice.

In this study, form-stable stearic acid-lauric acid/expanded perlite (SA-LA/EP) composite PCM was prepared by absorbing SA-LA eutectic mixtures into the pores of EP via vacuum impregnation. The microstructure, morphology and thermal properties and thermal stability of the composite PCMs were characterized by X-ray diffraction (XRD), scanning electron microscopy (SEM), Fourier transform infrared spectroscopy (FTIR), and thermogravimetric and differential scanning calorimetry. The structural stability and thermal reliability of the SA-LA/EP materials were evaluated in 100 melt-freeze cycles. The gypsum-based wallboards were prepared by incorporating the SA-LA/EP in different mass fractions. The mechanical property and the heating preservation performance of the wallboards were also investigated.

2. Experimental

2.1. Materials

Stearic acid (SA, $C_{18}H_{36}O_2$) and lauric acid (LA, $C_{12}H_{24}O_2$) were analytically pure and supplied by Tianjin Kemiou Chemical Reagent Co. Ltd, China. EP from Henan Province (China) was dried at 90 °C for 24 h and sieved using a 74-μm sieve. Gypsum was produced by the Xiongshi Construction Material Plant, China.

2.2. Preparation of expanded perlite composite PCMs

The melting temperatures of SA and LA were high. SA-LA eutectic mixtures were thus prepared to decrease the melting temperature. A series of SA and LA binary systems with different mass fractions were prepared to determine the optimum eutectic mixture ratio. SA-LA eutectic mixtures were slowly cooled to ambient temperature from liquid mixtures and the melting temperatures were obtained by an analysis of their cooling curves. The melting temperature data were plotted as a function of the composition and the eutectic mixture ratio and melting temperatures were determined by the intersection point of the temperature curves (Fig. 1a). Mixtures of SA and LA with a mass ratio of 3:7 were placed in a thermostated water bath at 90 °C for complete melting. The samples were stirred for 30 min and cooled to obtain the SA-LA eutectic mixtures. The melting temperature of the eutectic mixtures was about 30 °C, which is appropriate to the wall temperature in tropical regions. These mixtures were then used for the preparation of SA-LA/EP composite PCMs.

The SA-LA/EP composite PCMs were prepared by vacuum impregnation. One hundred grams of a SA-LA eutectic and 25.0 g EP were placed in a conical flask and the air pressure of the conical flask was maintained at −0.1 MPa for 30 min. The conical flask was then placed in a thermostated water bath at 90 °C for 1 h. The vacuum pump pressure was then reduced. The pressure of the conical flask was atmospheric pressure and this was maintained for 5 min. The composites were thermally filtered at 90 °C for 24 h to remove the redundant SA-LA eutectic mixtures. The mass of composites decreased because of the seepage of melted SA-LA from the composite PCMs. The mass of composites did not decrease longer as the duration of the thermal filter after 24 h, which indicated that the melted SA-LA leaked from the composites were removed entirely. The SA-LA leaked from the composites were gathered and weighed. The maximum SA-LA mass fraction (%) in the EP was calculated from the formula: the maximum SA-LA mass fraction (%) = $(m_0 - m)/(m_t - m) \times 100\%$, where m_0 was the initial mass of SA-LA in composites, m was the mass of SA-LA leaked from the composites and m_t was the total mass of composites. The SA-LA eutectic mixtures that were used for the PCMs were absorbed into the pores of the EP. The maximum SA-LA mass fraction in the EP was found to be 65%. The composites were regarded as form-stable composite PCMs because the melted SA-LA could not leak from the composite PCMs.

A thermal cycling test was conducted to investigate the thermal reliability of the SA-LA/EP form-stable composite PCMs. The sample was added to a test tube, which was put into a thermostated water bath at 90 °C. After the temperature of the sample reached 90 °C, the test tube was removed and cooled to ambient temperature. The test was carried out for 100 thermal cycles.

2.3. Characterization of expanded perlite composite PCMs

A thermogravimetric (TG) analysis of the SA-LA/EP was carried out at a heating rate of 10 °C/min up to 800 °C under nitrogen flow at atmospheric pressure. α-Al_2O_3 crucibles were used in a SDT Q600 instrument (TA Instrument-Waters LLC, New Castle, DE, USA). Differential scanning calorimetry (DSC) was conducted at a heating rate of 1 °C/min under a constant stream of argon at atmospheric pressure using a NETZSCH DSC 200 F3 Maia instrument (Selb, Germany, accuracy ±0.10 °C and ±1% for phase change temperatures and latent heat capacities, respectively). Powder X-ray diffraction (XRD) measurements of the samples were recorded on a DX-2700 X-ray diffractometer using Cu Kα radiation (λ=0.15406 nm) at a scan rate of 0.02 °/s and at 40 kV and 40 mA. The microstructures of the samples were investigated using a JEOL JSM-6360LV scanning electron microscope (SEM) at an accelerating voltage of 5 kV. FTIR spectra of the samples were obtained between 4000 cm^{-1} and 400 cm^{-1} on a Nicolet Nexus 670 FTIR spectrophotometer using KBr pellets. The mixtures were pressed into pellets for the IR measurements. To evaluate the pore structures of the expanded perlite, nitrogen gas adsorption-desorption isotherms were obtained at 77 K using an ASAP 2020 surface area analyzer (Micromeritics Co. Ltd.).

2.4. Preparation and performance evaluation of the wallboards

The gypsum used consisted primarily of β-$CaSO_4 \cdot 0.5H_2O$ (>85 %), and 90 % of particle size was less than 0.20 mm. The performance

parameters of gypsum included initial setting time (280 s), final setting times (530 s) and softening coefficient (0.33). The water/gypsum mass ratio and the dry procedure were determined by measuring the flexural strength of the wallboards. The flexural strengths of the wallboards with different water/gypsum mass ratio of 0.45, 0.50, 0.55 and 0.60 were 2.04, 2.76, 2.34 and 1.93 MPa after drying at 90 °C for 24 h, respectively. The flexural strengths of the wallboards after drying at 90 °C for different time of 6, 12, 24 and 48 h were 1.32, 1.85, 2.76 and 2.81 MPa with water/gypsum mass ratio of 0.50, respectively. Therefore, the optimized water/gypsum mass ratio (0.50) and dry procedure (90 °C for 24 h) were determined. The SA-LA/EP form-stable composite PCMs were blended at mass fractions of 2%, 4%, and 6%, respectively, and the mass ratio of water to gypsum was 0.50. All the raw materials were stirred uniformly and then cast into 100×100×100 mm^3 plastic molds. The SA-LA/EP wallboards were obtained after drying at 90 °C for 24 h. The EP wallboards were prepared as reference samples using the same processes. The thermal performance of the wallboards was determined using an in-house heating setup. As shown in Fig. 5a, the self-designed heating setup[41] consisted of an insulation box (350×200×200 mm^3), a 275 W infrared lamp, a constant heat board and temperature recorder. The wallboard sample was on the constant heat board, which was maintained at about 50 °C. The temperature recorder was fixed on the outer surface of wallboard sample to monitor the temperature change with time. The flexural strength of the wallboards was determined using a universal testing machine (CMT-5305, China).

3. Results and discussion

3.1. Characterization of the form-stable SA-LA/EP composite PCMs

The main factors for the selection of porous materials for packaging PCMs were pore structure characteristics such as the pore diameter distribution, the pore shape, and the porosity. The pore size distribution showed that the pore structure of the EP consisted of mesopores and macropores (inset of Fig. 1b). The nitrogen adsorption-desorption isotherms of the EP are of type IV (Fig. 1b). This indicates that both the mesopores and the macropores conform to the IUPAC classification. The specific surface area of the EP was 19.07 m^2/g and its total pore volume was 0.0114 cm^3/g. The pore size distribution of the EP in the mesoporous range was between 5 and 1000 nm (inset of Fig. 1b). The pore size of the EP presented trimodal distribution at 30, 49 and 85 nm. The honeycomb connected pores of the EP were obtained for rapid vaporization of structure water after perlite was treated at high temperatures. The pore structure and characteristics of the EP were suitable for adsorption and encapsulation of organic PCMs. Because of the large specific surface area and the pore volume, the EP had a high adsorption capacity for SA-LA because of capillary and surface tension forces.

The morphology of the EP and the SA-LA/EP form-stable composite PCMs are shown in the obtained SEM images (Fig. 1c,d). The EP possesses a honeycomb structure and many communicating pores (Fig. 1c). The diameters of the macropores are about 5–15 μm. The porous structure of the EP prevented the leakage of melted PCMs from the composites by capillary and surface tension forces. It also provided good mechanical strength to the composites. A comparison of the SEM images of the EP and the SA-LA/EP showed that the SA-LA eutectic mixtures were successfully absorbed into the pores of the EP. The porous morphology of the EP was not clear (Fig. 1d), indicating that the attachment and not the absorbent SA-LA was removed by the thermal filter. Therefore, the loading obtained using this condition was the maximum.

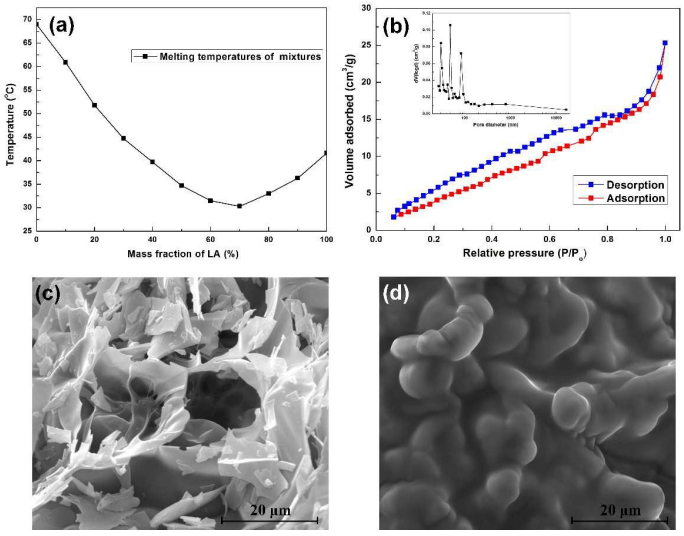

Fig 1. (a) Melting temperatures of SA-LA eutectic mixtures versus mass fraction of LA. (b) Nitrogen adsorption-desorption isotherms and BJH pore size distribution (inset) of expanded perlite. SEM images of (c) EP and (d) SA-LA/EP composite PCMs

XRD patterns of the raw materials and the SA-LA/EP composite PCMs are shown in Fig. 2a. The EP had an obvious broad diffraction peak at about 23° indicating that the EP mainly possessed an amorphous silica structure. The SA had three main diffraction peaks at about 6.80°, 21.52°, and 23.80°, and the LA had five main diffraction peaks at about 8.70°, 19.26°, 19.92°, 23.44°, and 24.40°. Therefore, the SA and the LA had good crystalline structures. In the XRD pattern of SA-LA the main SA and LA diffraction peaks became weaker because of the formation of SA-LA eutectic mixtures. It is clear that the main diffraction peaks of SA-LA/EP are similar to those of SA-LA and no new diffraction peaks are present. Therefore, the crystallization state of the SA-LA filled EP was well preserved and stable. The EP, as a porous supporting material, did not influence the crystal structure of SA-LA.

The compositions and the specific interactions of the composites were studied by FTIR spectroscopy. The FTIR spectra of SA, LA, SA-LA, EP, and SA-LA/EP are shown in Fig. 2b. For the SA-LA sample the absorption peaks at 2918 cm^{-1} and 2849 cm^{-1} correspond to the C–H stretching vibrations of $–CH_2$ and $–CH_3$, respectively. The broad absorption peak located at 3300–2800 cm^{-1} is assigned to the –OH stretching vibration and it overlaps the $–CH_2$ and $–CH_3$ stretching vibrations. The sharp absorption peak at 1703 cm^{-1} is caused by C=O stretching vibrations. The absorption peak at 1466 cm^{-1} corresponds to $–CH_2$ and $–CH_3$ deformation vibrations and the peak at 723 cm^{-1} comes from the rocking vibration of $–CH_2$. The adsorption peak at 1296 cm^{-1} is attributed to the in-plane bend

vibration of functional O–H and the peak at 935 cm^{-1} comes from the out-of-plane bending vibration of O–H groups. The FTIR spectrum of the LA is similar to that of the SA and the adsorption peaks of the SA and the LA at 2918, 2849, 1703, 1466, 1296, 935, and 723 cm^{-1} all appear in the FTIR spectrum of the SA-LA. The FTIR spectrum of the EP has a Si–O–Si asymmetric stretching vibration at 1092 cm^{-1} and a Si–O stretching vibration at 455 cm^{-1}. The peaks at 3626 cm^{-1} represent the asymmetric stretching vibration of the –OH functional group of Si–OH, and the absorption peaks at 787 cm^{-1} come from the SiO–H vibration.

Compared with the SA-LA, the SA-LA/EP composites had slightly shifted main peaks. The peak for the C=O stretching vibration shifted from 1703 to 1712 cm^{-1} and the peak of the O–H functional groups shifted from 935 to 943 cm^{-1}. The frequency shifts of the main groups indicate that physical interactions existed between the COOH group of the SA-LA and the alkaline region (SiO_2, CaO, Na_2O, and K_2O) of the EP[26]. The SA-LA absorbed easily into the pores of the EP because of these physical interactions and the leakage of melted SA-LA from the porous structure of the EP was thus prevented. No significant new peak was observed, indicating that there was no chemical reaction between the LA-SA and the EP. The binding features between expanded perlite and acid mixtures were mainly physical interaction such as van der Waals forces and hydrogen bonding, which had little effect on the crystallization of acid mixtures during the phase change process. Therefore, the acid mixtures had high crystallinity and adsorption capacity without leakage.

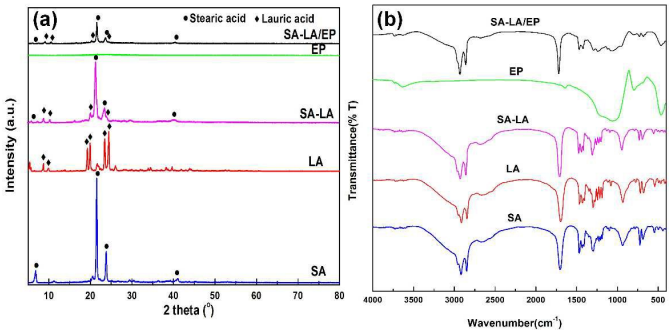

Fig 2. (a) XRD patterns and (b) FTIR spectra of SA, LA, SA-LA, EP and SA-LA/EP composite PCMs.

3.2. Thermal properties of the form-stable SA-LA/EP composite PCMs

The thermal properties (phase change temperatures and latent heat capacity) of the SA-LA and the SA-LA/EP composite PCMs were determined by DSC thermal analysis. From the DSC curves (Fig. 3a), the phase change temperatures for melting and freezing were found to be 31.27 °C and 29.89 °C for the SA-LA eutectic mixture, and 31.69 °C as well as 30.01 °C for the SA-LA/EP composite PCMs, respectively. The results showed that the SA-LA had a degree of subcooling (1.38 °C) and the phase change temperatures of the SA-LA/EP increased slightly. The extent of subcooling in the SA-LA/EP (1.68 °C) was slightly larger than that of the SA-LA. The minor changes in the phase change temperatures probably came from the interaction between the SA-LA and the pore wall of the EP and this is in good agreement with the FTIR results. However, the latent heats of melting and freezing were found to be 222.3 J/g and 222.5 J/g for the SA-LA eutectic mixture and 119.0 J/g as well as 117.4 J/g for the SA-LA/EP composite PCMs, respectively. The latent heat values of the SA-LA/EP were 54 % of that of the SA-LA eutectic mixture, while the loadage of SA-LA in the SA-LA/EP was about 65 wt.%. The latent heat values of the SA-LA/EP were lower than the theoretical values based on the mass ratio of the SA-LA in the composite PCMs. This was because the crystallizing of SA-LA eutectic mixture was hindered for the interactions between SA-LA and EP. The crystallinity of SA-LA in the composite was calculated to be 82.53 %[30].

From the TG and DTG curves of the SA-LA/EP composite PCMs (Fig. 3b), no apparent decomposition reaction or weight loss were found from 25 to 150 °C and the SA-LA/EP had excellent thermal stability below 150 °C. The rapid weight loss from 150 to 290 °C is related to SA-LA evaporation. The weight loss for the SA-LA/EP composite PCMs below 290 °C was 72.16 wt.%. This is approximately the mass fractions of SA-LA in the SA-LA/EP. The design working temperature for energy conservation in buildings is typically less than 80 °C and the SA-LA/EP composite PCMs can thus be used repeatedly.

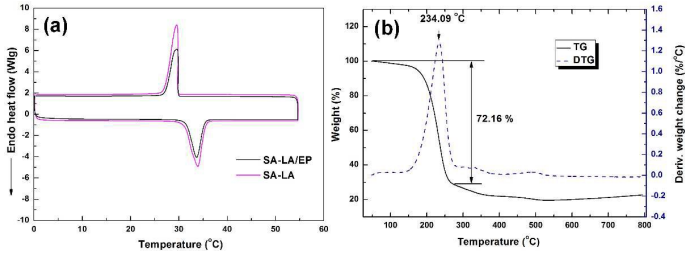

Fig 3. (a) DSC curves of SA-LA and SA-LA/EP composite PCMs. (b) TG and DTG curves of SA-LA/EP composite PCMs.

The phase change temperatures of the form-stable SA-LA/EP composite PCMs are suitable for LHTES purposes in buildings. This will increase human comfort and reduce energy consumption by decreasing the frequency of internal air temperature swings. The thermal properties of the SA-LA/EP composite PCMs were compared with those of different composite PCMs (Table 1) [26, 41, 43-48]. The latent heats of the SA-LA/EP composite PCMs that were prepared in this study are higher than those of other composite PCMs. This is attributed to the higher absorption capacity of the EP and the latent heat of the SA-LA. Therefore, form-stable SA-LA/EP composite PCMs are potentially important materials for building energy conservation.

3.3. Thermal reliability of the form-stable SA-LA/EP composite PCMs

Thermal reliability is an important parameter for composite PCMs and it plays a significant role in energy conservation in buildings. Composite PCMs should retain a stable chemical

state and structure after long-term use. The thermal reliability of the form-stable SA-LA/EP composite PCMs was evaluated by a properties comparison of the SA-LA/EP before and after thermal cycling.

Table 1 Comparison of thermal properties SA-LA/EP composite PCMs prepared with that of some composite PCMs in literatures.

Composite PCMs	Latent heat (J/g)	Melting point (°C)	Freezing point (°C)	References
Capric-stearic acid/gypsum	49.0	23.8	23.9	[43]
Capric acid/ halloysite	75.5	29.3	25.3	[44]
Paraffin/diatomite	70.5	47.8	44.2	[41]
Capric-palmitic acid/attapulgite	48.2	21.7	—	[45]
Capric–myristic acid/vermiculite	27.0	19.8	17.1	[46]
Lauric acid/ expanded perlite	93.4	44.1	40.9	[26]
Capric acid/ expanded perlite	98.1	31.8	31.6	[47]
Capric-myristic acid/ expanded perlite	85.4	21.7	20.7	[48]
SA-LA/EP	119.0	31.7	30.0	This work

The XRD patterns of the SA-LA/EP composite PCMs before and after thermal cycling are similar (Fig. 4a). Therefore, the impact of thermal cycling on the crystal structure of the SA-LA/EP composite PCMs was negligible. From the FTIR spectra of the SA-LA/EP composite PCMs before and after thermal cycling (Fig. 4b), none of the frequencies or shapes of the absorption peaks changed obviously after 100 thermal cycles. These results indicate that repeated melting/freezing cycling does not affect the chemical structure or interactions of the SA-LA/EP composite PCMs. The SEM images of the SA-LA/EP composite PCMs before and after thermal cycling are similar (Fig. 4c) and the outline of the EP became clearer after thermal cycling. This might be because of thermal cycling not changing the morphology of the SA-LA/EP but only removing the surface attached SA-LA on the EP. Therefore, the form-stable SA-LA/EP composite PCMs have stable chemical structures even after 100 thermal cycles.

To determine the thermal stability of the form-stable composite PCMs, a DSC thermal analysis of the SA-LA/EP composite PCMs after thermal cycling was carried out. From the DSC curves (Fig. 4d), the phase change temperatures for melting and freezing were determined to be 32.19 °C and 29.85 °C for the SA-LA/EP after thermal cycling. Its latent heats of melting and freezing were found to be 119.3 J/g and 116.8 J/g, respectively. A double peak was observed during the heating stage for the SA-LA/EP after thermal cycling. The similar trend was also found in other composite PCMs, and the low heating rate (1 °C/min) for DSC measurement made the trend more obvious, which may be associated with part SA-LA eutectic mixture absorbed into the micropores (< 5 nm) of EP during the thermal cycling. The movement and crystallizing of the SA-LA eutectic mixture in the micropores were confined, and its crystallinity and melting temperature were slightly lower than that of the SA-LA eutectic mixture in the mesopores and macropores. So, the little peak on the left could be assigned to the phase change of the SA-LA eutectic mixture in the micropores, and the major peak was greatly attributed to the phase change of the SA-LA eutectic mixture in the mesopores and macropores. After 100 melting/freezing cycles, the phase change temperatures for melting and freezing of the SA-LA/EP changed by 1.58% and -0.53%, respectively, and the latent heats of melting and freezing changed by 0.25% and -0.51%, respectively. The changes of the latent heats of melting and freezing of the SA-LA/EP after thermal cycling were comparable to current other composite PCMs, such as paraffin/expanded vermiculite composite[27] (-0.37% and 0.94%), Stearic acid/kaolin composite[50] (1.16% and 0.46%), and polyethylene glycol/graphene[51] (-2.09% and -3.06%) poly vinyl chloride microencapsulated PCMs[52] (-12.85% and -3.28%). These results show that the phase change temperature and the latent heat did not change significantly. Therefore, the form-stable SA-LA/EP composite PCMs have stable thermal properties even after 100 thermal cycles. The thermal reliability of the form-stable SA-LA/EP composite PCMs thus meets the application requirements of energy conservation in buildings.

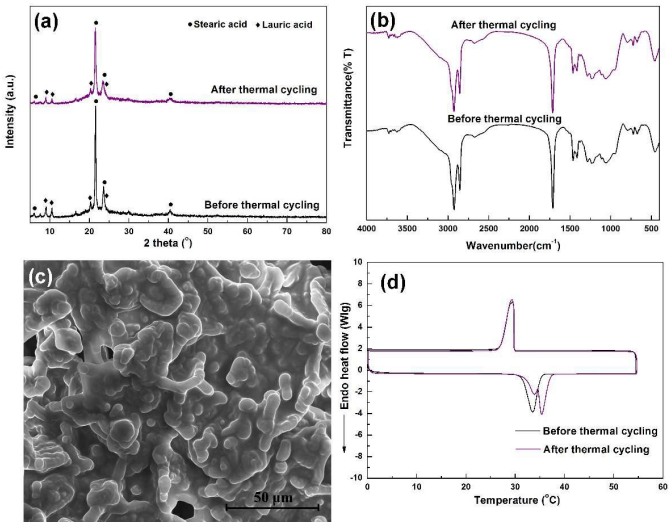

Fig 4. (a)XRD patterns, (b) FTIR spectra and (d) DSC curves of SA-LA/EP composite PCMs before and after 100 thermal cycling. (c) SEM images of SA-LA/EP composite PCMs after 100 thermal cycling.

3.4. Mechanical and thermal performances of the wallboards

Gypsum-based heat preservation wallboards were prepared using different mass fractions of SA-LA/EP or EP. The physical and thermal properties of the wallboards were thus determined (Table 2). As far as density is concerned, the SA-LA/EP wallboards were

found to be the lightest followed by the EP wallboards. The density of the wallboards decreased with an increase in SA-LA/EP or EP mass fraction. Therefore, the SA-LA/EP wallboards are better adapted to the light weight requirement of modern buildings. The flexural strength of the wallboards decreased with an increase in mass fraction and the flexural strength of the SA-LA/EP wallboards decreased the most. This was because the gypsum content was reduced and the skeleton bonding function of gypsum weakened. The reduced flexural strength of the SA-LA/EP wallboards is still acceptable for many building applications and conforms to relevant standards for building materials.

Table 2 Physical and thermal properties of building wallboards.

Sample		Density (g/cm^3)	Flexural strength (MPa)	Temperature at 500s (°C)	Temperature at 1000s (°C)
Sample name	Fraction (wt.%)				
Gypsum wallboards	0	1.157	2.76	31.3	34.4
EP wallboards	2	1.142	2.52	30.2	32.7
	4	1.141	2.37	28.9	31.9
	6	1.141	2.23	28.7	31.7
SA-LA/EP wallboards	2	1.116	2.48	30.0	32.3
	4	1.014	2.32	28.8	31.8
	6	0.924	2.19	28.1	29.7
Heat storage cement mortar [53]		1.406	2.01	—	—
Ordinary cement mortar [53]		1.635	2.31	—	—
Gypsum standards of China		≤1.100	≥2.10	—	—

The thermal performance of the wallboards was evaluated by determining the temperature change with time using an in-house heating setup (Fig. 5a). A thermal performance comparison between the SA-LA/EP wallboards and gypsum wallboards is shown in Fig. 5b. Compared with the gypsum wallboards, the SA-LA/EP wallboards have an obviously lower surface temperature after heating for 1500 s. The temperature of the SA-LA/EP wallboards tended to stabilize at about 30 °C while that of the gypsum wallboards tended to stabilize at about 35 °C. The wallboard temperatures obtained at 500 s and 1000 s are listed in Table 2. The heat preservation performance of the SA-LA/EP wallboards was best followed by the EP wallboards. The heat preservation performance of the wallboards decreased with an increase in the mass fraction of the SA-LA/EP or the EP. Therefore, the gypsum-based SA-LA/EP wallboards have potential application in the heating preservation of interior walls in buildings. The composite PCMs with melting point of about 30 °C were suitable for application in the building thermal insulation in hot regions with large temperature difference between day and night, such as inland areas close to desert. The highest daytime temperatures in these regions were generally higher than 35 °C in summer, while the nighttime temperatures dropped below 23 °C. The composite PCMs could store thermal energy and stabilize the indoor temperatures at about 30 °C during the day, and release thermal energy against the cold at night. Therefore, the composite PCMs could reduce the indoor temperature swing and save the building energy consumption.

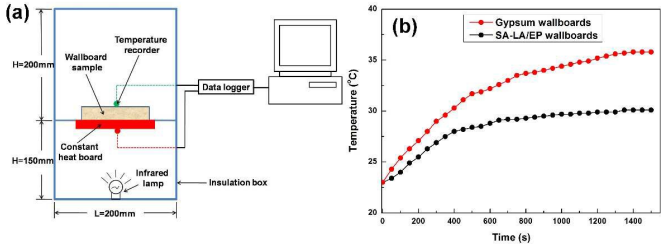

Fig 5. (a) Schematic of self-designed heating setup. (b) Thermal performance comparison between SA-LA/EP wallboards and gypsum wallboards.

4. Conclusions

Form-stable SA-LA/EP composite PCMs were prepared by the vacuum impregnation of SA-LA eutectic mixtures into porous EP. The maximum mass fraction of SA-LA confined in the EP was 65% without the seepage of melted SA-LA from the composite PCMs and the composites can be described as form-stable. These results show that SA-LA is absorbed into the pores of EP by physical interactions. The phase change temperature and the latent heats of the SA-LA/EP upon melting and freezing were determined to be 31.69 °C, 30.01 °C, 119.0 J/g, and 117.4 J/g, respectively. The form-stable SA-LA/EP composite PCMs had excellent structural stability and thermal reliability after 100 thermal cycles. The wallboards prepared using SA-LA/EP and gypsum had low density, acceptable mechanical strength, and remarkable heating preservation performance. The form-stable SA-LA/EP composite PCMs may be used in wallboards and have important potential advantages in terms of building energy conservation because of their excellent thermal properties, their satisfactory mechanical properties, their simple preparation process, and their low cost.

Acknowledgements

This work was supported by the National Science Fund for Distinguished Young Scholars (51225403), the Specialized Research Fund for the Doctoral Program of Higher Education (20120162110079), the State Key Laboratory of Powder Metallurgy, Central South University, and the Hunan Provincial Co-Innovation Centre for Clean and Efficient Utilization of Strategic Metal Mineral Resources.

Notes and references

1. A. M. Omer, *Renew. Sust. Energ. Rev.*, 2008, **12**, 2265-2300.
2. L. Pérez-Lombard, J. Ortiz and C. Pout, *Energy Build.*, 2008, **40**, 394-398.

3. C. Scheuer, G. A. Keoleian and P. Reppe, *Energy Build.*, 2003, **35**, 1049-1064.
4. I. Sartori and A. G. Hestnes, *Energy Build.*, 2007, **39**, 249-257.
5. B. Tashtoush, M. Molhim and M. Al-Rousan, *Energy*, 2005, **30**, 1729-1745.
6. K. F. Fong, V. I. Hanby and T. T. Chow, *Energy Build.*, 2006, **38**, 220-231.
7. L. Lu, W. Cai, L. Xie, S. Li and Y. C. Soh, *Energy Build.*, 2005, **37**, 11-22.
8. D. Zhang, J. Zhou, K. Wu and Z. Li, *Sol. Energy*, 2005, **78**, 471-480.
9. F. Kuznik, D. David, K. Johannes and J.-J. Roux, *Renew. Sust. Energ. Rev.*, 2011, **15**, 379-391.
10. S. A. Memon, *Renew. Sust. Energ. Rev.*, 2014, **31**, 870-906.
11. A. M. Khudhair and M. M. Farid, *Energy Conv. Manag.*, 2004, **45**, 263-275.
12. A. Shukla, D. Buddhi and R. L. Sawhney, *Renew. Energy*, 2008, **33**, 2606-2614.
13. M. K. Rathod and J. Banerjee, *Renew. Sust. Energ. Rev.*, 2013, **18**, 246-258.
14. S. B. Stanković and P. A. Kyriacou, *Appl. Energy*, 2013, **109**, 433-440.
15. A. I. Fernandez, M. Martínez, M. Segarra, I. Martorell and L. F. Cabeza, *Sol. Energy Mater. Sol. Cells*, 2010, **94**, 1723-1729.
16. M. M. Farid, A. M. Khudhair, S. A. K. Razack and S. Al-Hallaj, *Energy Conv. Manag.*, 2004, **45**, 1597-1615.
17. W. Wang, X. Yang, Y. Fang and J. Ding, *Appl. Energy*, 2009, **86**, 170-174.
18. C. Alkan and A. Sari, *Sol. Energy*, 2008, **82**, 118-124.
19. K. Lin, Y. Zhang, X. Xu, H. Di, R. Yang and P. Qin, *Energy Build.*, 2005, **37**, 215-220.
20. A. Sarı, *Energy Conv. Manag.*, 2004, **45**, 2033-2042.
21. J. Li, P. Xue, W. Ding, J. Han and G. Sun, *Sol. Energy Mater. Sol. Cells*, 2009, **93**, 1761-1767.
22. A. Sarı, C. Alkan and A. Karaipekli, *Appl. Energy*, 2010, **87**, 1529-1534.
23. L. Wang and D. Meng, *Appl. Energy*, 2010, **87**, 2660-2665.
24. A. Sarı and A. Karaipekli, *Sol. Energy Mater. Sol. Cells*, 2009, **93**, 571-576.
25. A. Karaipekli, A. Sarı and K. Kaygusuz, *Renew. Energy*, 2007, **32**, 2201-2210.
26. A. Sarı, A. Karaipekli and C. Alkan, *Chem. Eng. J.*, 2009, **155**, 899-904.
27. C. Li and H. Yang, *J. Am. Ceram. Soc.*, 2013, **96**, 2793-2798.
28. B. Xu and Z. Li, *Energy*, 2014, **72**, 371-380.
29. S. Song, L. Dong, Y. Zhang, S. Chen, Q. Li, Y. Guo, S. Deng, S. Si and C. Xiong, *Energy*, 2014, **76**, 385-389.
30. C. Li, L. Fu, J. Ouyang and H. Yang, *Sci. Rep.*, 2013, **3**, 1-8.
31. A. M. Goitandia, G. Beobide, E. Aranzabe and A. Aranzabe, *Sol. Energy Mater. Sol. Cells*, 2015, **134**, 318-328.
32. J. Deng, W. Li and D. Jiang, *Sust. Dev. Urban Environ. Build. Mater.*, 2012, **374-377**, 807-810.
33. D. Xu and H. Yang, *Funct. Mater. Lett.*, 2014, **07**, 1440011.
34. S. Liu and H. Yang, *Energy Technol.*, 2015, **3**, 77-83.
35. N. Tekin, E. Kadıncı, Ö. Demirbaş, M. Alkan, A. Kara and M. Doğan, *Micropor. Mesopor. Mater.*, 2006, **93**, 125-133.
36. İ. B. Topçu and B. Işıkdağ, *Build. Environ.*, 2007, **42**, 3540-3546.
37. Z. Lu, J. Zhang, G. Sun, B. Xu, Z. Li and C. Gong, *Energy*, 2015, **82**, 43-53.
38. D. Sun, L. Wang and C. Li, *Mater. Lett.*, 2013, **108**, 247-249.
39. Z. Lu, B. Xu, J. Zhang, Y. Zhu, G. Sun and Z. Li, *Sol. Energy*, 2014, **108**, 460-466.
40. N. Zhang, Y. Yuan, Y. Yuan, T. Li and X. Cao, *Energy Build.*, 2014, **82**, 505-511.
41. B. Xu and Z. Li, *Appl. Energy*, 2013, **105**, 229-237.
42. M. Li, Z. Wu and M. Chen, *Energy Build.*, 2011, **43**, 2314-2319.
43. A. Sarı, A. Karaipekli and K. Kaygusuz, *Int. J. Energy Res.*, 2008, **32**, 2.
44. D. Mei, B. Zhang, R. Liu, Y. Zhang and J. Liu, *Sol. Energy Mater. Sol. Cells*, 2011, **95**, 2772-2777.
45. M. Li, Z. Wu and H. Kao, *Appl. Energy*, 2011, **88**, 3125-3132.
46. A. Karaipekli and A. Sarı, *Sol. Energy*, 2009, **83**, 323-332.
47. A. Sarı and A. Karaipekli, *Mater. Chem. Phys.*, 2008, **109**, 459-464.
48. A. Karaipekli and A. Sarı, *Renew. Energy*, 2008, **33**, 2599-2605.
49. S. Karaman, A. Karaipekli, A. Sarı and A. Biçer, *Sol. Energy Mater. Sol. Cells*, 2011, **95**, 1647-1653.
50. S. Liu and H. Yang, *Appl. Clay. Sci.*, 2014, **101**, 277-281.
51. G. Qi, J. Yang, R. Bao, Z. Liu, W. Yang, B. Xie and M. Yang, *Carbon*, 2015, **88**, 196-205.
52. H. Zhang, Y. Zou, Y. Sun, L. Sun, F. Xu, J. Zhang and H. Zhou, *Sol. Energy Mater. Sol. Cells*, 2015, **137**, 210-218.
53. M. Li, Z. Wu and J. Tan, *Appl. Energy*, 2013, **103**, 393-399.